An SDR-Based Monostatic Wi-Fi System with Analog Self-Interference Cancellation for Sensing

Andreas Toftegaard Kristensen*, Alexios Balatsoukas-Stimming†, and Andreas Burg*
*Telecommunication Circuits Laboratory, École polytechnique fédérale de Lausanne, Switzerland
†Eindhoven University of Technology, The Netherlands

arXiv:2412.08612v1 [eess.SP] 11 Dec 2024

***Abstract*—Wireless sensing offers an alternative to wearables for contactless monitoring of human activity and vital signs. However, most existing systems use bistatic setups, which suffer from phase imperfections due to unsynchronized clocks. Monostatic systems overcome this issue, but are hindered by strong self-interference (SI) that require effective cancellation. We present a monostatic Wi-Fi sensing system that uses an auxiliary transmit RF chain to achieve SI cancellation levels of 40 dB, comparable to existing solutions with custom cancellation hardware. We demonstrate that the cancellation filter weights, fine-tuned using least-mean squares, can be directly repurposed for target sensing. Moreover, we achieve stable SI cancellation over 30 minutes in an office environment without fine-tuning, enabling traditional vital sign monitoring using channel estimates derived from baseband samples without the adaptation of the cancellation affecting the sensing channel – a significant limitation in prior work. Experimental results confirm the detection of small, slow-moving targets, representative for breathing chest movements, at distances up to 10 meters in non-line-of-sight conditions.**

***Index Terms*—ISAC, device-free sensing, RF sensing, monostatic sensing, Wi-Fi sensing, openwifi, SI cancellation.**

I. Introduction

Real-time, continuous monitoring of human activity and vital signs, particularly heart and respiratory rates, is crucial for enhancing healthcare analytics and early detection of health issues [1–4]. However, wearable technologies face limitations such as user discomfort and non-compliance [5, 6]. An ideal monitoring system would enable contactless, continuous data collection with minimal discomfort for the user. Recognizing these challenges, researchers have focused on developing wireless contact-free monitoring systems using common technologies such as Wi-Fi. Most Wi-Fi sensing systems extract channel information from commodity devices, avoiding specialized hardware [7–11]. However, these systems operate in bistatic mode, with physically separated transmitters and receivers, which face challenges due to unsynchronized transmitter and receiver clocks, causing imperfections such as carrier frequency offset (CFO), sampling frequency offset (SFO), and sampling time offset (STO) that severely impair sensing performance. While calibration methods can partially mitigate these issues [12], they also lead to information loss and potential distortion of the sensing signal. In contrast, monostatic setups avoid the synchronization issues, but face other challenges like self-interference (SI), which necessitate self-interference cancellation (SIC) strategies similar to those in full-duplex (FD) radio systems [13]. Without proper handling, the strong SI can mask targets, cause receiver nonlinearities, and lead to analog-to-digital converter (ADC) saturation as the SI is orders of magnitude stronger than the sensing signal [14, 15]. To mitigate SI for both sensing and communication, various SIC techniques have been explored. Direct radio frequency (RF) cancellation methods rely on analog electronics that tap into the RF signal from the transmit (Tx) chain to train and drive a canceller. By directly accessing the output of components like power amplifiers (PAs), direct RF cancellers avoid explicitly modeling potential non-idealities, but complex custom cancellation hardware is still needed to adapt the cancellation signal [14]. A simpler approach in terms of the hardware is to use an auxiliary Tx path, where the SIC signal is digitally generated using a secondary Tx port for RF cancellation [16–18]. However, as this auxiliary Tx path does not have access to the RF SI signal, it may have to explicitly model non-idealities, e.g., from the PA to achieve a sufficient level of SIC. While this may seemingly put auxiliary Tx cancellation systems at a disadvantage compared to direct RF cancellation systems, which are also more common for sensing [15, 19–22], we demonstrate in this work that the auxiliary approach can provide sufficient SIC. Another consideration for cancellation systems is the calibration and updating/tracking of the cancellation parameters. If the canceller is frequently fine-tuned to track variations in the system hardware, SIC remains high, but the target is also suppressed [15, 19–22]. Proposed mitigation approaches include fitting the canceller to the near environment (a few meters) and only sensing distant targets [15], performing Doppler-based sensing for large, fast-moving objects between fine-tuning periods [19, 20], or only training the canceller on the direct path SI using an antenna switch to remove the multipath [21, 22].

Contributions: We present a fully software-defined radio (SDR)-based monostatic Wi-Fi setup with an auxiliary transmit RF chain for SIC, significantly simplifying the hardware requirements compared to previous works that focus on custom analog electronics for SIC. We demonstrate that our analog self-interference cancellation (AnSIC) setup achieves SIC comparable to similar setups and that our cancellation is stable over 30 minutes without fine-tuning the AnSIC filter weights. Based on this setup, we demonstrate the re-purposing of the AnSIC filter weights for sensing, enabling sensing information recovery at the same time as continuously fine-turning the AnSIC filter weights, which to the best of our knowledge has not been shown before. Finally, we demonstrate the ability to sense a small slow-moving target at a distance of $10\,\mathrm{m}$ in non-line-of-sight (NLOS) using the residual signal when keeping the filter weights fixed over an extended time period.

TABLE I: AnSIC and openwifi FPGA area consumption.

	LUT	FF	BRAM	DSP
AnSIC	8,495	9,983	0	80
openwifi	36,258	50,446	126	107

II. Background

In this section, we first describe the wireless sensing model and then we explain how our AnSIC filter is trained.

A. Wi-Fi Sensing

For Wi-Fi sensing, while the channel frequency response (CFR) is commonly employed, the channel impulse response (CIR) often proves superior as it concentrates sensing information into fewer delay bins, thus reducing feature dimensionality [23, 24]. The CIR can be expressed as

$$g(t,\tau) = \sum_{p=1}^{P} \alpha_p(t)\rho(\tau - \tau_p(t))e^{-j2\pi f_c \tau_p(t)}\,, \qquad (1)$$

where $\rho(\tau) = \frac{\sin(\pi B\tau)}{\pi B\tau}$ is the pulse shape function, P is the number of multipath components, α_p is the coefficient of path p, $\tau_p(t)$ is the delay of path p, B is the signal bandwidth, and f_c is the carrier frequency. The CIR obtained from a wireless device is a sampled CIR vector $\mathbf{g}$, with entries $g[n] = g\left(\frac{n}{B}\right)$.

For a monostatic system, the CIR can be decomposed into

$$g(t,\tau) = g_{\mathrm{i}}(t,\tau) + g_{\mathrm{s}}(t,\tau) + g_{\mathrm{d}}(t,\tau)\,, \qquad (2)$$

where $g_{\mathrm{i}}(t,\tau)$, $g_{\mathrm{s}}(t,\tau)$, and $g_{\mathrm{d}}(t,\tau)$ represent the channels originating from the SI, static scatterers, and dynamic scatterers, respectively. Note that for a more compact notation, we omit the dependency on time t and delay τ in the following.

B. Self-Interference and AnSIC fitting

The auxiliary Tx path model for AnSIC is composed of two paths, with an antenna path for one digital-to-analog converter (DAC) and a cancellation path for a second DAC. In the antenna path, baseband in-phase and quadrature (I/Q) samples x pass through h_{delay} (for an n-cycle delay), $h_{\text{tx},0}$ (transmit channel), $h_{\text{ch},0}$ (wireless channel), and h_{rx} (receive channel). With only the antenna path active, the received signal is r_0, which represents the SI signal. In the cancellation path, x passes through h_{filt} (AnSIC filter), $h_{\text{tx},1}$, and $h_{\text{ch},1}$, yielding r_1 without h_{filt} and r_{filt} with it. When both paths are active with the AnSIC filter, the received signal is given as r_{canc}

$$r_{\text{canc}} = h_{\text{rx}} * (x * h_{\text{delay}} * h_0 + x * h_{\text{filt}} * h_1)\,. \qquad (3)$$

where $*$ denotes convolution and $h_i = h_{\text{tx,i}} * h_{\text{ch,i}}$. To fit h_{filt}, we derive the least mean squares (LMS) update rule for the N-tap filter $\mathbf{h}_{\text{filt}}$. In vector-notation, for the n-th discrete time-step, the filter state is $\mathbf{h}_{\text{filt}}[n]$ and the measured residual SI is $r_{\text{canc}}[n]$. The task of the AnSIC filter is to filter the transmitted baseband samples $\mathbf{x}[n] \in \mathbb{C}^N$ such that the transmitted signals from each port cancel each other out at an RF combiner. As a cost function, we use $C[n] = |e[n]|^2$ with $e[n] = r_{\text{canc}}[n]$. The gradient wrt. $\mathbf{h}_{\text{filt}}$ is given as $\nabla_{\mathbf{h}_{\text{filt}}} C[n] = \mathbf{r}_1^*[n]e[n]$. The filter update rule is

$$\mathbf{h}_{\text{filt}}[n+1] = \mathbf{h}_{\text{filt}}[n] - \mu\nabla_{\mathbf{h}_{\text{filt}}} C[n] = \mathbf{h}_{\text{filt}}[n] - \mu\mathbf{r}_1^*[n]e[n]\,, \quad (4)$$

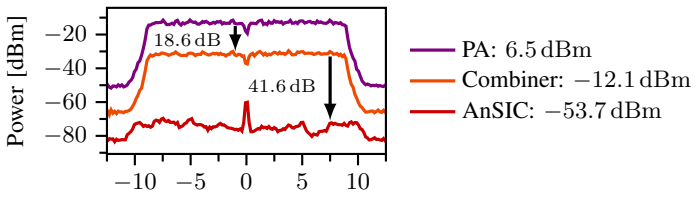

Fig. 1: Power measurements at different stages of the RF chain. The carrier frequency is 2.472 GHz.

where μ is the learning rate. This update process utilizes r_1, rather than x, to account for the effect of the cancellation path. Therefore, r_1 has to be measured. This is done by transmitting only on the RF port used for the cancellation and collecting the receive (Rx) baseband samples on the shared Rx port. However, we later demonstrate that r_1 does not have to be measured often as the cancellation path is highly stable.

III. Analog Self-Interference Cancellation

In this section, we first describe the hardware used for our AnSIC filter. Then, we present its performance.

A. Hardware for Self-Interference Cancellation and Sensing

Our testbed is based on a modified version of the openwifi project, an open-source IEEE 802.11 Wi-Fi SDR implemented on a Xilinx XC7Z020-CLG484 field-programmable gate array (FPGA) [24–26]. The AD-FMCOMMS2-EBZ RF front-end provides two Rx and two Tx chains. For monostatic sensing, the system transmits and receives simultaneously, with a shared local oscillator for the Tx and Rx paths, eliminating the CFO, STO, and SFO impairments. The shared Tx/Rx antenna path includes a CN0417 PA board (∼20 dB gain) [27], a MECA CS-2.5000 circulator (∼13 dB attenuation) [28], a Mini-Circuits VBF-2435+ bandpass filter (2,340 −2,530 MHz) [29], and a Mini-Circuits ZX10-2-252-S+ splitter [30] to combine the paths for the shared ADC. The orthogonal frequency-division multiplexing (OFDM) signal bandwidth is 20 MHz. This setup requires only one additional RF port, the auxiliary Tx port, and uses off-the-shelf components, eliminating the need for custom printed circuit board (PCB) and electronics design. In contrast, similar monostatic systems with AnSIC [15, 19–22] often require sophisticated custom analog hardware and PCBs.

B. AnSIC Filter Area Consumption

Table I presents the FPGA area consumption separately for the AnSIC filter and the openwifi system. The AnSIC filter processes 16-bit I/Q samples using 16-bit weights, with a filter length of 20. The system operates with a 40 MHz clock. While the FPGA is small, both the openwifi system and the AnSIC filter fit, enabling the use of small and relatively cheap FPGAs. Note that the AnSIC filter is fitted on the CPU.

C. Signal Spectrum Characteristics with AnSIC

We validate the AnSIC performance using measurements obtained using a Rohde & Schwarz FS315 [31] spectrum analyzer. For the measurements, we use a Tx port memory

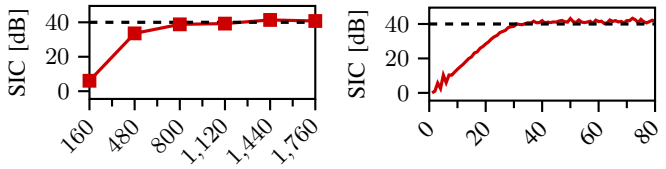

(a) LS SIC vs. I/Q sample count. (b) SIC vs. number of LMS steps.

Fig. 2: SIC as a function of (a) the number of I/Q samples for LS and (b) the number of LMS steps, respectively.

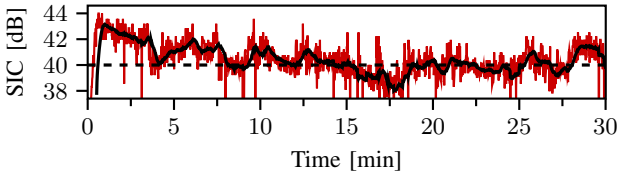

Fig. 3: Red indicates the 10 Hz SIC measurements and black the SIC moving average over 30 s.

buffer to continuously transmit a Wi-Fi frame with no gaps in between the frame transmissions to ensure accurate power measurements. The buffer contains a Wi-Fi frame of 3920 I/Q samples, which is also used for least squares (LS) fitting. Rx and cancellation port gains are pre-calibrated and the automatic gain control (AGC) disabled.

Fig. 1 shows the signal spectrum at the PA output after the RF combiner with and without the AnSIC filter. Without AnSIC, the power level at the RF combiner output is -12.1 dBm. After applying AnSIC with a LS-fitted filter, the power reduces to -53.7 dBm, indicating a 41.6 dB cancellation. The residual signal after AnSIC shows $\sim$10 dB variation across the 20 MHz bandwidth, indicating low frequency selectivity. This contrasts with the electrical balance duplexer (EBD) setup in [19], which exhibits up to 20 dB variation across the same bandwidth. As noted in [16], EBDs generally show higher frequency selectivity than other cancellation techniques. The systems in [22] and [15] demonstrate similarly low frequency selectivity to our results. Our setup can achieve $\sim$42 dB, aligning well with the literature [15, 19–22]. With the 13 dB of isolation from the circulator, and not accounting for the bandpass filter and RF combiner, we achieve 55 dB of isolation.

D. AnSIC Performance for LS and LMS Fitting

This section evaluates the requirements in terms of number of I/Q samples for LS and LMS to fit AnSIC filter weights. Fig. 2a illustrates the SIC improvement as a function of the number of I/Q samples used for LS fitting. The SIC significantly improves from 160 to 480 samples and plateaus around 1440 samples (72 µs of air-time). 40 dB of SIC is achieved with 800 samples (40 µs of air-time), indicating high SIC can be achieved with short Wi-Fi frame segments. While LS is effective for initial training, LMS is more suitable for channel tracking. For LMS fitting, 80 I/Q samples from the high throughput long training field (HT-LTF) field are used, representing 4 µs. The same r_1 measurement is reused across all training iterations. Fig. 2b shows convergence in about

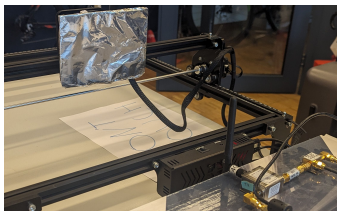

(a) CNC-machine for AnSIC filter weight sensing.

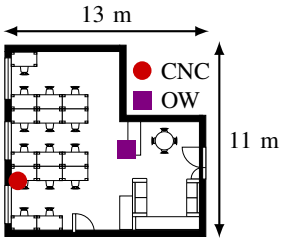

(b) Floorplan with openwifi (OW) and computer numerical control (CNC) location.

Fig. 4: Photo and floorplan of the setup used for the AnSIC filter sensing test (a) and the NLOS CIR sensing test (b).

40 LMS steps (128 µs of air-time). When executed on the CPU, the training rate can reach up to $\sim$500 Hz when fitting based on 80 I/Q samples. The reuse of r_1 for several LMS steps underscores the cabled cancellation path stability and demonstrates that it is not necessary to re-measure r_1 for every filter update, simplifying the process of fine-tuning.

E. Long-Term Stability of AnSIC

A 30 minute experiment was conducted in a populated office environment to evaluate the AnSIC stability. Following initial LMS fitting, Rx power measurements were collected at 10 Hz on the openwifi board. Fig. 3 illustrates the ability of our system to maintain an average SIC of $\sim$40 dB throughout most of the 30 minute experiment. This consistent performance indicates stable Tx paths after initial fitting, with no significant drifts between the two Tx paths. A brief SIC degradation occurred around 15 min, but the system recovered to 42 dB cancellation by the end of the experiment. Our system thus maintains robust cancellation despite occasional interference. The work demonstrates potential for long-term SIC stability without frequent retraining, contrasting with monostatic setups in [19, 20] that continuously retrain, and [15, 21, 22] where the retraining frequency is unclear or unspecified during sensing.

IV. Results - Sensing

In this section, we evaluate our system for sensing. We discuss two approaches: first we adapt the filter weights continuously and use the changing weights for sensing. Then, we fix the AnSIC weights and perform sensing based on the residual signal.

A. Sensing with AnSIC Filter Weights

When $\mathbf{h}_{\text{filt}}$ is fine-tuned to the channel, it contains information on all components in (2), including the dynamic (g_{d}) ones. We demonstrate this using the experimental setup in Fig. 4a, which uses a CNC machine with an aluminum foil covered plate (8 cm $\times$ 12 cm) to emulate breathing. The CNC machine moves 1 cm at 12 breaths per minute (bpm) to emulate human breathing [32] and 20 cm to evaluate performance under stronger interference, aligning with related works [15, 19–22] that focus on larger and faster-moving targets. 12 bpm is chosen as it corresponds to the smallest value in the 12 to 15 bpm range for human breathing at rest [33, p. 588].

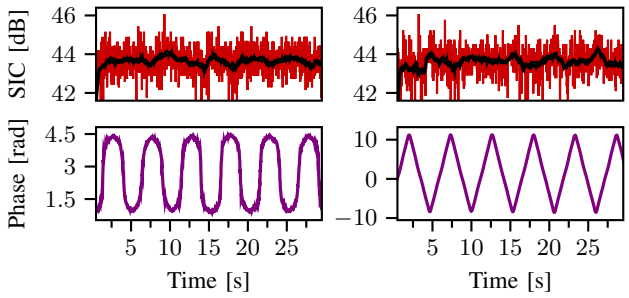

Fig. 5: SIC (top) and filter weight (zero-meaned) phase (bottom) with LMS and CNC movement. 1 s SIC moving average.

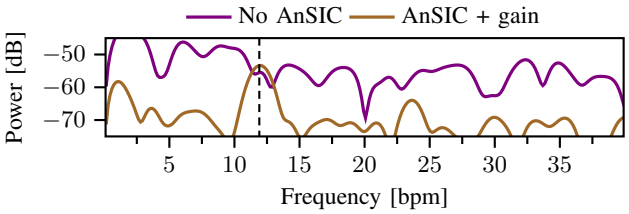

Fig. 6: Frequency spectrum for the 50 ns CIR delay bin.

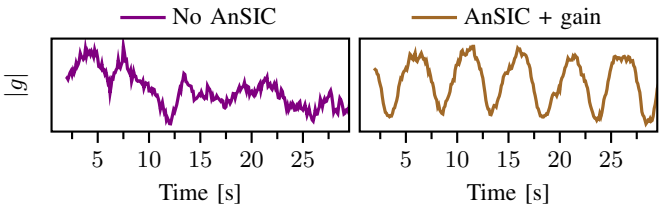

Fig. 7: Magnitude for the 50 ns CIR delay bin over 30 s.

The SIC results in Fig. 5 show that our AnSIC filter maintains ∼44 dB SIC in both scenarios, indicating effective real-time adaptation. While real-time adaption has also been demonstrated in [19, 20] where the SIC is stable under close movements, we further demonstrate the ability to perform sensing based on the filter coefficients as shown in Fig. 5. The phase of the main AnSIC filter weight clearly represents the periodic movement of the CNC machine, indicating real-time adaptation to changing interference patterns. While [20] also demonstrates a similar use of cancellation filter weights for sensing, they use a digital canceller.

B. CIR-Based Sensing

To perform sensing on the residual SI, we also consider the CIR estimated from the residual received signal when the AnSIC filter is fixed after initial LS-fitting. CIR-based sensing experiments were conducted in a lab space (Fig. 4b) using the same CNC machine as before (Fig. 4a) to again emulate human breathing. To make detection more challenging, we consider a NLOS scenario, with the openwifi board and CNC locations in Fig. 4b. This scenario has a 10 m direct path, but the target is not visible from the position of the openwifi board and is hidden behind a lab desk setup. The CNC machine moves 1 cm at 12 bpm to emulate breathing.

For AnSIC, the board was configured as described in Section III-A. When AnSIC is disabled, the cancellation port is attenuated to prevent noise through the combiner. Wi-Fi frames of 3920 I/Q samples were transmitted at 100 Hz for 1 minute. The Rx I/Q collection is triggered by the transmission of the first sample from the FPGA. To estimate the CIR, we extracted all OFDM symbols from the I/Q samples, computed the CIR for each OFDM symbol, and then averaged these across all symbols within each frame. The data was resampled to 10 Hz for a uniform sampling rate. As the OFDM bandwidth is 20 MHz, the CIR delay resolution is 25 ns or 7.5 m. We define the 0 ns delay bin as the one with the highest power, representing the direct path SI. As the target is at distance of 10 m in NLOS conditions, we expect the target to show up around the 25 ns or 50 ns delay bins, corresponding to distances of 7.5 m and 15 m. When analyzing all delay bins in the frequency domain, the 50 ns bin was found to be the strongest at 12 bpm. Hence, we focus on this bin.

Frequency-Domain: Fig. 6 shows the spectrum of the 50 ns bin for 1 min of measurements. For the frequency spectra, the curve is shifted down for the Rx gain increase. Without AnSIC, no distinct peak at 12 bpm is observed, indicating difficulty in estimating slow targets under SI. Applying AnSIC recovers a strong peak at 12 bpm and enables an Rx gain increase of ∼40 dB from the Rx power reduction. These findings highlight the challenges of NLOS sensing and the necessity of SI mitigation techniques, with AnSIC to effectively reduce the impact of SI and optimize Rx gain and ADC utilization.

Time-Domain: Fig. 7 shows the magnitude of the 50 ns bin. No clear periodic signal is visible without AnSIC. With AnSIC, Fig. 7 reveals a clear signal, although some distortion remains. These results, in alignment with the frequency domain findings, demonstrate that with AnSIC, sensing targets can be recovered at a distance of 10 m in NLOS conditions.

V. Conclusion

In this paper, we presented an SDR-based monostatic Wi-Fi sensing system that employs an auxiliary AnSIC approach. Our system achieves SIC levels comparable to existing solutions while simplifying hardware requirements. We have demonstrated that unlike previous works [15, 19–22] our setup preserves sensing information in two ways. First, the AnSIC filter weights can be used directly for sensing with LMS fine-tuning. Second, the stability of the cancellation, allows for long periods without fine-tuning the filter while maintaining a high level of SIC. This enables sensing from received I/Q samples and allow for traditional vital sign sensing using channel estimates derived from baseband samples without interference from the canceller's adaptation – a significant improvement over previous systems that require careful consideration of the effect of the fine-tuning when performing sensing. Our experiments confirmed the ability of our system to detect small, slow-moving targets at distances of up to 10 m in NLOS conditions. These findings indicate that effective SIC and accurate sensing in monostatic systems can be achieved without custom hardware and with stable performance.

Acknowledgment

This research has been kindly supported by the Swiss National Science Foundation under Grant-ID 182621.

References

[1] S. S. Gambhir, T. J. Ge, O. Vermesh, and R. Spitler, "Toward achieving precision health," *Science Translational Medicine*, vol. 10, no. 430, p. eaao3612, 2018.

[2] Y. Khan, A. E. Ostfeld, C. M. Lochner, A. Pierre, and A. C. Arias, "Monitoring of vital signs with flexible and wearable medical devices," *Advanced materials*, vol. 28, no. 22, pp. 4373–4395, 2016.

[3] M. H. Ebell, "Predicting pneumonia in adults with respiratory illness," *American family physician*, vol. 76, no. 4, pp. 560–562, 2007.

[4] K. Fox, J. S. Borer, A. J. Camm, N. Danchin, R. Ferrari, J. L. Lopez Sendon, P. G. Steg, J.-C. Tardif, L. Tavazzi, M. Tendera *et al.*, "Resting heart rate in cardiovascular disease," *Journal of the American College of Cardiology*, vol. 50, no. 9, pp. 823–830, 2007.

[5] A. Ometov, V. Shubina, L. Klus, J. Skibińska, S. Saafi, P. Pascacio, L. Flueratoru, D. Q. Gaibor, N. Chukhno, O. Chukhno, A. Ali, A. Channa, E. Svertoka, W. B. Qaim, R. Casanova-Marqués, S. Holcer, J. Torres-Sospedra, S. Casteleyn, G. Ruggeri, G. Araniti, R. Burget, J. Hosek, and E. S. Lohan, "A Survey on Wearable Technology: History, State-of-the-Art and Current Challenges," *Computer Networks*, vol. 193, p. 108074, 2021.

[6] H. Jeong, H. Kim, R. Kim, U. Lee, and Y. Jeong, "Smartwatch wearing behavior analysis: a longitudinal study," *Proceedings of the ACM on Interactive, Mobile, Wearable and Ubiquitous Technologies*, vol. 1, no. 3, pp. 1–31, 2017.

[7] D. Halperin, W. Hu, A. Sheth, and D. Wetherall, "Tool release: Gathering 802.11n traces with channel state information," *ACM SIGCOMM Computer Communication Review*, vol. 41, no. 1, p. 53, 2011.

[8] Y. Xie, Z. Li, and M. Li, "Precise power delay profiling with commodity WiFi," in *Proceedings of the 21st Annual International Conference on Mobile Computing and Networking*, ser. MobiCom '15. ACM, 2015, pp. 53–64.

[9] F. Gringoli, M. Schulz, J. Link, and M. Hollick, "Free your CSI: A channel state information extraction platform for modern Wi-Fi chipsets," in *Proceedings of the 13th International Workshop on Wireless Network Testbeds, Experimental Evaluation & Characterization - WiNTECH '19*. ACM Press, 2019.

[10] Z. Jiang, T. H. Luan, X. Ren, D. Lv, H. Hao, J. Wang, K. Zhao, W. Xi, Y. Xu, and R. Li, "Eliminating the barriers: Demystifying Wi-Fi baseband design and introducing the PicoScenes Wi-Fi sensing platform," *arXiv:2010.10233 [cs]*, 2021.

[11] F. Gringoli, M. Cominelli, A. Blanco, and J. Widmer, "AX-CSI: Enabling CSI extraction on commercial 802.11ax Wi-Fi platforms," in *Proceedings of the 15th ACM Workshop on Wireless Network Testbeds, Experimental Evaluation & CHaracterization*. ACM, 2022, pp. 46–53.

[12] Y. Zeng, D. Wu, J. Xiong, E. Yi, R. Gao, and D. Zhang, "FarSense: Pushing the range limit of WiFi-based respiration sensing with CSI ratio of two antennas," *Proceedings of the ACM on Interactive, Mobile, Wearable and Ubiquitous Technologies*, vol. 3, no. 3, pp. 1–26, Sep. 2019.

[13] M. Duarte and A. Sabharwal, "Full-duplex wireless communications using off-the-shelf radios: Feasibility and first results," in *2010 Conference Record of the Forty Fourth Asilomar Conference on Signals, Systems and Computers*. IEEE, Nov. 2010, pp. 1558–1562.

[14] D. Korpi, "Full-duplex wireless: Self-interference modeling, digital cancellation, and system studies," 2017.

[15] C. B. Barneto, T. Riihonen, M. Turunen, L. Anttila, M. Fleischer, K. Stadius, J. Ryynänen, and M. Valkama, "Full-Duplex OFDM Radar With LTE and 5G NR Waveforms: Challenges, Solutions, and Measurements," *IEEE Transactions on Microwave Theory and Techniques*, vol. 67, no. 10, pp. 4042–4054, Oct. 2019.

[16] L. Laughlin, C. Zhang, M. A. Beach, K. A. Morris, and J. Haine, "A widely tunable full duplex transceiver combining electrical balance isolation and active analog cancellation," in *2015 IEEE 81st Vehicular Technology Conference (VTC Spring)*. IEEE, May 2015, pp. 1–5.

[17] A. Kiayani, M. Abdelaziz, D. Korpi, L. Anttila, and M. Valkama, "Active RF Cancellation with Closed-Loop Adaptation for Improved Isolation in Full-Duplex Radios," in *2018 IEEE Globecom Workshops (GC Wkshps)*. Abu Dhabi, United Arab Emirates: IEEE, Dec. 2018, pp. 1–6.

[18] A. Kiayani, M. Z. Waheed, L. Anttila, M. Abdelaziz, D. Korpi, V. Syrjälä, M. Kosunen, K. Stadius, J. Ryynänen, and M. Valkama, "Adaptive Nonlinear RF Cancellation for Improved Isolation in Simultaneous Transmit-Receive Systems," *IEEE Transactions on Microwave Theory and Techniques*, vol. 66, no. 5, pp. 2299–2312, May 2018.

[19] S. A. Hassani, V. Lampu, K. Parashar, L. Anttila, A. Bourdoux, B. van Liempd, M. Valkama, F. Horlin, and S. Pollin, "In-Band Full-Duplex Radar-Communication System," *IEEE Systems Journal*, vol. 15, no. 1, pp. 1086–1097, Mar. 2021.

[20] S. A. Hassani, B. Van Liempd, A. Bourdoux, F. Horlin, and S. Pollin, "Joint In-Band Full-Duplex Communication and Radar Processing," *IEEE Systems Journal*, vol. 16, no. 2, pp. 3391–3399, Jun. 2022.

[21] Z. Chen, T. Zheng, C. Hu, H. Cao, Y. Yang, H. Jiang, and J. Luo, "ISACoT: Integrating Sensing with Data Traffic for Ubiquitous IoT Devices," *IEEE Communications Magazine*, pp. 1–7, 2022.

[22] Z. Chen, C. Hu, T. Zheng, H. Cao, Y. Yang, Y. Chu, H. Jiang, and J. Luo, "ISAC-Fi: Enabling Full-fledged Monostatic Sensing over Wi-Fi Communication," *IEEE Journal of Selected Areas in Sensors*, pp. 1–15, 2024.

[23] S. Li, A. T. Kristensen, A. Burg, and A. Balatsoukas-Stimming, "ComplexBeat: Breathing rate estimation from complex CSI," in *2021 IEEE Workshop on Signal Processing Systems (SiPS)*. IEEE, 2021, pp. 217–222.

[24] A. T. Kristensen, S. Li, A. Balatsoukas-Stimming, and A. Burg, "Monostatic Multi-Target Wi-Fi-Based Breathing Rate Sensing Using Openwifi," in *2024 IEEE Wireless Communications and Networking Conference (WCNC)*. Dubai, United Arab Emirates: IEEE, Apr. 2024, pp. 1–6.

[25] X. Jiao, W. Liu, M. Mehari, H. Thijs, and A. Muhammad. (2023) open-source ieee802.11/wi-fi baseband chip/fpga design. [Online]. Available: https://github.com/open-sdr

[26] X. Jiao, W. Liu, M. Mehari, M. Aslam, and I. Moerman, "Openwifi: A free and open-source IEEE802.11 SDR implementation on SoC," in *2020 IEEE 91st Vehicular Technology Conference (VTC2020-Spring)*. IEEE, May 2020, pp. 1–2.

[27] Analog Devices, "CN0417 Evaluation Board Guide," https://www.analog.com/en/resources/reference-designs/circuits-from-the-lab/cn0417.html, accessed: 2024-08-19.

[28] MECA Electronics, "CS-2.5000 Circulator: 2.3 - 2.7 GHz, 20 Watts, SMA," https://e-meca.com/products/cs-2-500-m03-20-watts-sma-female-2-3-2-7-ghz, accessed: 2024-08-19.

[29] Mini-Circuits, *VBF-2435+ LTCC Band Pass Filter, 2340 - 2530 MHz, 50 Ohm*, 2024, rev. G, Accessed: 2024-08-28. [Online]. Available: https://www.minicircuits.com/WebStore/dashboard.html?model=VBF-2435%2B

[30] ——, "ZX10-2-252-S+ Splitter: 500 - 2500 MHz, 50 Ohm, SMA," https://www.minicircuits.com/WebStore/dashboard.html?model=ZX10-2-252-S%2B, accessed: 2024-08-19.

[31] *R&S FS315 Operating Manual*, Rohde & Schwarz, 2024, accessed: 2024-08-19. [Online]. Available: https://www.rohde-schwarz.com/us/manual/r-s-fs315-operating-manual-manuals_78701-29352.html

[32] A. Boussuges, Y. Gole, and P. Blanc, "Diaphragmatic motion studied by M-mode ultrasonography," *Chest*, vol. 135, no. 2, pp. 391–400, 2009.

[33] K. E. Barrett and W. F. Ganong, *Ganong's Review of Medical Physiology*, 23rd ed. New York: McGraw-Hill Medical, 2010.